Positron-electron pairs emitted from metallic and oxide surfaces

I. S. Brandt,[1] Z. Wei,[1] F. O. Schumann,[1,*] and J. Kirschner[1,2]
[1]*Max Planck Institut für Mikrostrukturphysik, Weinberg 2, 06120 Halle, Germany*
[2]*Institut für Physik, Martin-Luther Universität, 06120 Halle, Germany*
(Received 24 March 2015; revised manuscript received 4 August 2015; published 6 October 2015)

If a positron impacts onto a surface, it may lead to the emission of a positron-electron pair. We have commissioned a laboratory-based positron source and performed a systematic study on a variety of solid surfaces. In a symmetric emission geometry we can explore the fact that positrons and electrons are distinguishable particles. Following fundamental symmetry arguments we have to expect that the available energy is shared unequally among positrons and electrons. Experimentally we observe such a behavior for all materials studied. We find a universal feature for all materials in the sense that, on average, the positron carries a larger fraction of the available energy. A scattering model accounts qualitatively for the observed energy sharing in positron-electron pair emission. A comparison of the intensity levels from the different materials reveals a monotonic relation between the singles and pair coincidence count rates.

DOI: 10.1103/PhysRevB.92.155106 PACS number(s): 73.20.At, 79.60.−i

I. INTRODUCTION

Ferromagnetism has been known to mankind for centuries and an explanation of this phenomenon has eluded classical physics as stated in the Bohr-van Leuwen theorem. The introduction of a new equation of motion, the Schrödinger equation, was necessary to provide a microscopic description of ferromagnetic order. Of key importance is the notion of indistinguishability of identical particles, which leads to the Pauli principle. In the case of spin-$\frac{1}{2}$ particles, it states that the many-body wave function has to be antisymmetric upon exchange. This principle explains the periodic table and it is the combination of the Pauli principle and the Coulomb interaction which favors an ordering of the magnetic moments in ferromagnets and antiferromagnets. This is usually referred to as the exchange interaction. In general, the microscopic interplay between the electrons via Coulomb interaction and exchange is the origin of the emergence of correlation effects in solids which have no counterpart in atomic physics.

Photoelectron spectroscopy has become a versatile tool to study the electronic properties of atoms, molecules, and solids. Correlation effects are known to show up in the spectra, but more insight can be gained if one detects two electrons in coincidence. This type of spectroscopy is called (e,2e) or double photoemission if the excitation is via a primary electron or photon, respectively. Due to the fact that two electrons are detected, the relations between them can be studied. This, in turn, makes it possible to infer the relations of the electrons within the solid. As a particular example, we refer to the angular relations between the emitted electrons. We have shown that this reveals the exchange-correlation (xc) hole [1–3]. This concept was introduced in the beginning of the 1930s by Wigner and Seitz and Slater [4,5] and plays a pivotal role in modern solid-state theory [6].

For a better understanding of correlation effects in solids, it is desirable to disentangle their individual contributions. To this end we have performed a spin-resolved (e,2e) study in which a spin-polarized electron beam impinges onto a ferromagnetic surface [7,8]. The relative orientation of the primary electron spin and the majority spin directions can be easily controlled. The differences in the angular distributions for parallel and antiparallel alignment demonstrated that it is possible to effectively separate exchange from Coulomb correlation. However, this approach requires a ferromagnetic sample. A variety of highly correlated materials display antiferromagnetic order; therefore, an alternative way has to be pursued.

If a primary positron hits a surface it can lead to the emission of a positron-electron pair, we term this process as (p,ep) [9,10]. Positrons and electrons are distinguishable; hence, the interaction between them does not include exchange. If one compares the angular (p,ep) distributions from those of (e,2e) experiments, it is also possible to separate the effect of exchange from the Coulomb correlation. The prospect of this approach was discussed in theoretical (p,ep) studies for surfaces [11,12]. In these calculations it was also shown that the (p,ep) energy distributions reveal the distinguishability between the positron and the electron.

In our previous work we demonstrated that the positron-electron pair production at surfaces leads to features in the energy distributions which are a consequence of distinguishable collision partners [10]. Specifically, we noticed that the energy sharing curves are asymmetric. In that work we employed a symmetric emission geometry via a normal incident positron beam and used fundamental symmetry arguments to predict such an outcome. These arguments cannot be used if the emission geometry is broken by a non-normal incident beam.

In the present work we discuss the outcome on the energy distributions. The comparison with the data obtained in normal incidence shows that the change in the symmetry hardly affects the energy spectra. We have studied a variety of materials and find a consistent behavior in the sense that the positron carries, on average, the larger part of the available energy. We also report on the singles and coincidence intensity levels for a variety of metals and NiO, which is usually considered as a highly correlated material. We discovered a systematic relation of the singles to the coincidence count rates. The pair production rate per primary positron for NiO is a factor 2–3 higher compared to the metals. The weak material dependence

*schumann@mpi-halle.de

of the energy distributions and material dependence of the coincidence rate can be explained within a simplified scattering model.

II. EXPERIMENT

Electron spectroscopy techniques are widely used in surface science, and excitation sources like electron guns or UV light sources are readily available. As far as excitation with primary positrons is concerned, a significant effort has to be made. The most common way for a laboratory source is the use of the ^{22}Na isotope which decays into Ne upon emitting a positron and a 1.27-MeV γ quantum. The radioactive isotope has a half-life of 2.6 yr. The energy spectrum is continuous with an end energy of 545 keV. The positron source was supplied by iThemba LABS within a standard capsule and has a γ activity of 50 mCi [13]. The capsule has a 5-μm-thick Ti window through which the positrons can pass [13]. In a test experiment we determined the total positron current, leaving the capsule and obtained a value of 66 pA. This amounts to an emission rate of 4.1×10^8 e^+/s, which is 23% of the γ activity.

In order to create a monoenergetic beam, the process of moderation is utilized [14]. It is based on the observation that for certain materials positron bombardment leads to the emission of low-energy positrons with a kinetic energy of a few eV albeit with a low probability. We use a tungsten mesh as moderator which has a reported efficiency of a few 10^{-4}. This means an upper bound of the flux onto the sample is of the order of several 10^4 moderated positrons per second.

In Fig. 1 we show some details of the positron moderation and the beam formation. In close proximity to the capsule one can find the W moderator made of a stack of eight meshes which is followed by a 90° spherical deflector. Only positrons with the correct kinetic energy, which is controlled by an applied voltage to the moderator, will traverse the deflector. Additional lens elements transport the positrons into the scattering chamber while unmoderated positrons and γ quanta are unaffected by the deflector. The moderator chamber is surrounded by a lead housing with a weight of 1 ton for radiation shielding. This positron optics system provides a flux of 3×10^4 positrons per second focused on an area of 5 mm diameter for positron energies in the range of 30–65 eV. This positron flux agrees with values obtained with similar setups utilized and is in line with the above-made estimate [15,16]. The pressure inside the positron optics system was 2×10^{-10} mbar. For additional electron-induced electron (e,2e) studies, we utilize a commercial electron gun with a BaO cathode.

The scattering experiments are performed in a UHV chamber, which is equipped with standard surface science tools like Auger spectroscopy and low-energy electron diffraction. Several electron beam evaporators are available for the deposition of metal and oxide films. The coincidence spectrometer has been explained in more detail elsewhere [17]. The key components are a pair of hemispherical analyzers with 200 mm mean radius, which we call "left" and "right" respectively. They are equipped with channel plates with resistive anodes as position-sensitive detectors to record the impact position. Depending on the polarity of the electron-optical potentials, detection of either electrons or positrons is chosen. The primary positron beam lies within the scattering plane as defined by the lens axes of the two spectrometers; see Fig. 2. The acceptance angle of the spectrometer lenses is ±15° within the scattering plane. For all experiments the analyzers were set to a pass energy of 300 eV. This results in a 27-eV-wide energy window which can be covered in parallel by each spectrometer.

The primary positron flux available is by a factor 100 lower than the flux usually employed for (e,2e) experiments used with the same instrument. A channel-plate detector can be brought into the sample position and makes it possible to determine the primary flux in the experiment. In order to compensate for the drop in count rate we had to increase the entrance slit width from 1 to 9 mm. This compromise leads to a significantly degraded energy resolution of 4 eV for each spectrometer. We employ a four-way coincidence circuit in which the channel-plate signals have to be within 135 ns, while at the same time the electronics of the resistive anodes

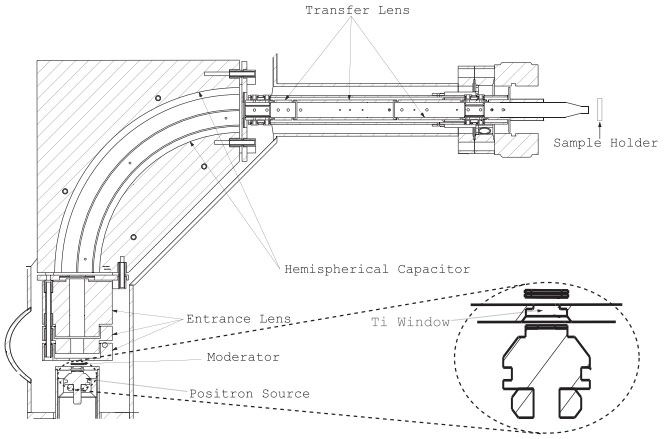

FIG. 1. Simplified diagram for the ^{22}Na e^+ source, moderator and beam transport. The source is in close proximity to the moderator, which reemits low-energy positrons. An entrance lens guides those particles into the hemispherical capacitor. Only positrons with the desired kinetic energy will arrive at the transfer lens, which will focus the positron beam onto the sample.

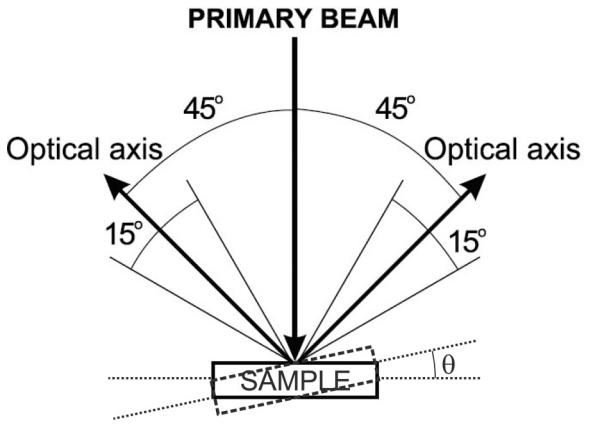

FIG. 2. The two transfer lenses of the spectrometer (with ±15° acceptance) are symmetrically aligned with respect to the primary beam. For normal incidence (polar angle $\theta = 0°$) a symmetric emission geometry is ensured.

indicate a successful impact position determination. The latter are needed to determine the kinetic energy of the coincident particles. For each valid event the arrival time ($t_{\rm left}$ and $t_{\rm right}$) at the respective detector with respect to the coincidence trigger is known. This makes it possible to compute the arrival time histogram $dt = t_{\rm left} - t_{\rm right}$ and this will show a peak residing on a constant background. The temporal width of the peak can be understood by electron-optical considerations of the actual spectrometer [17–19]. Following standard procedures it is possible to remove the aggregate effect of the "random" coincidences [17,20,21]. In the following we present energy spectra which have been corrected in this way.

The substrate was a single-crystal Ag(100) surface which was cleaned via Ar^+ sputtering and annealing. For the deposition of metal films *e*-beam evaporators were available. The preparation of NiO films on a Ag(100) substrate is well documented [22–27]. The Ni evaporation was performed in an O_2 atmosphere of 10^{-7} mbar. All coincidence experiments were carried out at room temperature.

III. KINEMATICS AND SIMPLIFIED SCATTERING MODEL

In Fig. 2 we sketch the geometric arrangement of our coincidence experiment. We performed two series of experiment for different values of the polar angle θ. The first set was performed for normal incidence of the positron beam ($\theta = 0^\circ$). The energy distributions for this geometry was the focus of our previous study [10]. The second series was obtained with $\theta = \pm 12^\circ$. For the normal incidence case the axis of the primary positron beam, the sample normal, and the lens axes of the left and right spectrometer form a symmetric arrangement.

Let us suppose that an electron pair is emitted in which the electrons posses different kinetic energies E_1 and E_2, respectively. The likelihood that the electron with energy E_1 is detected by the left spectrometer is identical to being registered by the right spectrometer, because electrons cannot be distinguished. This symmetry is broken if one of the spectrometers is sensitive to positrons while the other analyzes electrons. Consequently, we have to expect that the energy distributions of positron-electron pairs display a nonsymmetric behavior.

In a (p,ep) process, a primary positron with well-defined primary energy E_p impinges on the surface and a positron-electron pair is emitted. We introduce a notation in which the subscript indicates the spectrometer and a superscript refers to the polarity of the particle. If we label the kinetic energies as $E^+_{\rm left}$ and $E^-_{\rm right}$, we perform an experiment where the left spectrometer is sensitive to positrons while the right spectrometer detects electrons. If we label the polarity of the detected particles with α and β, energy conservation for a (p,ep) experiment reads as

$$E^p + E_{vb} = E^\alpha_{\rm left} + E^\beta_{\rm right} + \phi = E_{\rm sum} + \phi. \qquad (1)$$

We remove one electron from the sample; hence, the electron work function ϕ appears. The positron work function does not enter the energy balance, because the energy gained upon entering the surface is lost after the emission of the positron into the vacuum. The valence state participating in the scattering experiment has a binding energy given by E_{vb}, where the reference is the Fermi level E_F. The positron-electron pair has an energy sum $E_{\rm sum} = E^\alpha_{\rm left} + E^\beta_{\rm right}$, which has an upper bound given by $E^{\rm max}_{\rm sum} = E^p - \phi$. The energy balance for the (e,2e) process is formally identical to Eq. (1) if we set $\alpha = \beta = -$. In this case, E^p is the energy of the primary electron.

An additional kinematic variable concerns the momentum. The periodicity of the surface has important consequences for the conservation of the in-plane momentum, which is written as

$$\sin(\theta)k^p + k_{vb} = k^\alpha_{\rm left} + k^\beta_{\rm right} + g. \qquad (2)$$

The valence electron momentum is given by k_{vb} and the contribution of the primary positron depends on the polar angle θ. As can be seen from Fig. 2 the absolute value of θ cannot exceed 30° before the sample starts to reduce the acceptance of one spectrometer. We define the coordinate system such that particles detected by the right (left) spectrometer possess a positive (negative) in-plane momentum. The momenta of the emitted particles appear on the right-hand side of Eq. (2) together with the reciprocal lattice vector g. Super- and subscripts have the same meaning as Eq. (1).

For low-energy excitation the reciprocal lattice vector g can be ignored. Further simplification is possible if we consider normal incidence, as in Fig. 2, which leads to the following equation:

$$k_{vb} = k^\alpha_{\rm left} + k^\beta_{\rm right}. \qquad (3)$$

Usually the electronic density of states (DOS) is nonzero over a large part of the surface Brillouin zone. This fact makes it kinematically possible for positron and electron to possess different energies while having fixed emission angles of, say, ±45°, respectively. This is very different from a binary scattering of positron and electron, where emission angles of ±45° demand that both particles must have the same kinetic energy as we discuss below. Clearly, the existence of the crystal momentum is important for the kinematics. Nevertheless, we want to ignore the solid-state environment for the moment which reduces to a two-body problem.

In the laboratory frame the electron is initially at rest, while the primary positron approaches it with primary energy E_p. Afterwards the positron has lost part of its energy to the electron and is deflected by an angle ϑ from its original trajectory. The electron has a momentum direction characterized by an angle φ with respect to the momentum of the primary positron. Energy and momentum conservation uniquely define the energies of the two particles and the propagation direction of the electron for a given value of ϑ. In the case of particles with equal mass, it is easy to show that $\vartheta + \varphi = 90^\circ$. Furthermore, the maximum deflection angle ϑ is ±90°, which is obtained if the positron has vanishing kinetic energy after the scattering. Straightforward evaluation of the energy and momentum conservation leads to expressions of the kinetic energy of positron $E^+(\vartheta)$ and electron $E^-(\vartheta)$ after the collision. From this we compute the energy difference or energy sharing ΔE:

$$\Delta E = E^+(\vartheta) - E^-(\vartheta) = E_p \cos(2\vartheta). \qquad (4)$$

If the angle ϑ equals 45° the energy sharing ΔE is zero. This is very different from the scattering of a solid surface. In

other words, the binary collision is for the kinematics more restrictive than the surface scattering. The actual scattering problem is usually solved after transformation into the center-of-mass frame. For equal mass particles the relation between the scattering angles in the two reference frames is given by $\Theta = 2\vartheta$. This angle occurs already in the expression for ΔE; see Eq. (4). The actual scattering problem is solved once the scattering amplitude $f(\Theta)$ is obtained. With this knowledge the probability for a particular energy sharing to occur is given by $|f(\Theta)|^2$. The extreme values of the energy sharing are given by $\pm E_p$ as a consequence of Eq. (4).

We would like to provide a numerical example and recall that the theoretical description of the (p,ep) and (e,2e) process at solid metal surfaces assumes a screened Coulomb interaction $V \sim e^{(-r/\lambda)}/r$ between the collision partners [12,28,29]. In this expression the distance between the positron and electron is given by r, while the screening length is labeled with λ. We set the kinetic energy of the primary positron to 30 eV, while the screening length is 2 Å. This reflects values used in a (p,ep) calculation for a Cu(111) surface [12]. For further analysis we use the first Born approximation to determine the scattering amplitude $f(\Theta)$. We point out that the theoretical description [12,28,29] goes beyond the first Born approximation.

In Fig. 3(a) we present the resulting intensity as a function of the energy sharing. It is immediately obvious that the intensity distribution favors the positron to be the more energetic particle after the scattering. This fact is an immediate consequence of the scattering involving distinguishable particles.

It is instructive to perform the same analysis for the scattering of two electrons. In this case we have to ensure that the total wave function is antisymmetric upon exchange. We have to distinguish between two different spin orientations, namely singlet and triplet. For the singlet case we have to replace the scattering amplitude $f(\Theta)$ with $f(\Theta) + f(\pi - \Theta)$, whereas in the triplet case the expression $f(\Theta) - f(\pi - \Theta)$ is to be used [30]. In the case of an unpolarized primary electron beam and an unpolarized target, we have to calculate the statistical average of the two intensity distribution. In this case the sharing distribution is symmetric, as evidenced by Fig. 3(b). This probability of the sharing we use for the surface scattering without relating the angles ϑ and φ to the emission angles covered by the our spectrometers. This step takes into account the less stringent kinematics in the surface scattering, as discussed before. In a surface scattering experiment the angle of the incident primary particle is well defined, while in a binary collision this entity does not exist. Therefore, our prediction of the sharing distribution does not include a dependence of the angle of incidence.

A consequence of the binary scattering geometry is that in the laboratory frame both particles must have momentum components along the forward direction. This is clearly different from our experimental geometry, where the particles have momentum components along the backward direction. There has to be a mechanism for momentum reversal which turns out to be the effect of diffraction. It is a well-established fact that electrons are elastically backscattered from solid surfaces. This effect forms the basis of structural analysis of surfaces termed low-energy electron diffraction (LEED). The equivalent process using positrons exists and is termed low-energy positron

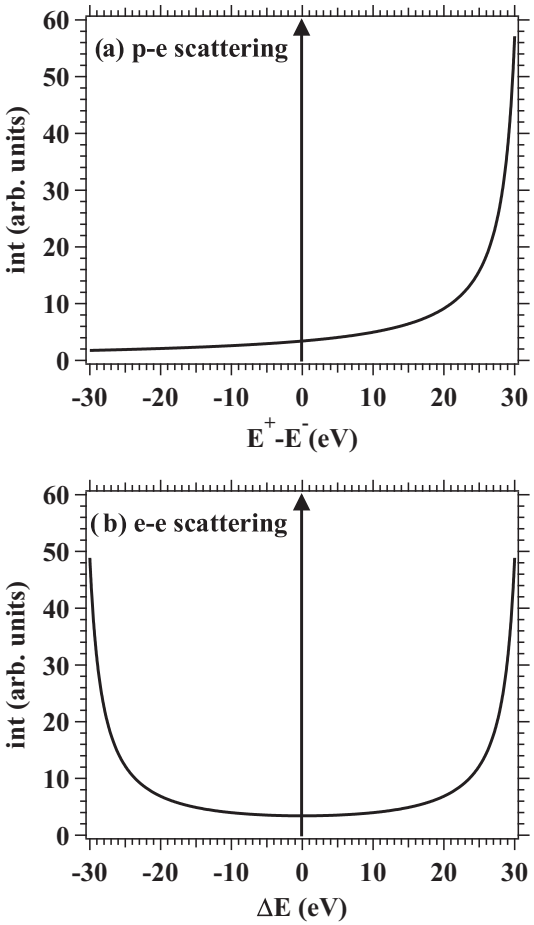

FIG. 3. We show the scattering intensity as a function of the energy sharing within a binary collision. The primary particle has an energy of 30 eV and the screening length of the Yukawa potential is 2 Å. In (a) we show the result for the positron-electron case, while in (b) the data for the electron-electron scattering are plotted.

diffraction (LEPD) [31–33]. Therefore, this reflected beam acts as the primary beam for the positron-electron scattering or electron-electron scattering from surfaces. An additional pathway of momentum reversal is that the positron-electron pair experiences diffraction. The diffraction of electron pairs has been observed in (e,2e) experiments [34–36].

At this point we recall the result of a (p,ep) calculation from a Cu(111) surface [12]. In this work the authors assumed an emission geometry similar to the one shown in Fig. 2 with emission directions of $\pm 30^\circ$. From this calculation we learn that the effect of distinguishability shows up through an unequal energy sharing between positron and electron. It depends on details of the electronic states whether the electron or the positron is, on average, the more energetic particle.

IV. RESULTS

A. Energy distributions for normal incidence

Before we present the energy distributions for non-normal incidence, it is appropriate to recall the the most important features for normal incidence. Following the discussion above, we have to expect a sharing curve which is asymmetric.

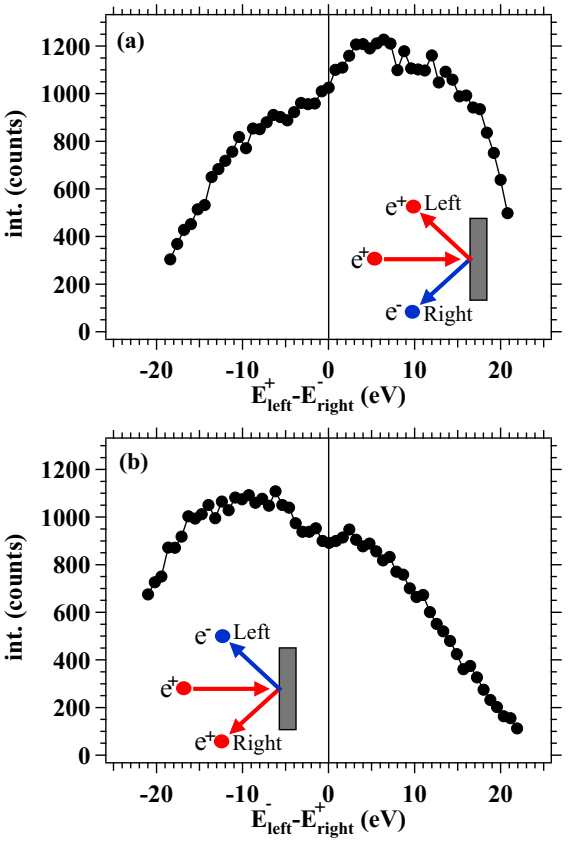

FIG. 4. (Color online) Energy sharing curves obtained by fixing the sum energy to 30 ± 2 eV. The Cu/Ag(100) sample was excited by 42 eV positrons. The insets indicate which of the particles is detected by the respective spectrometer.

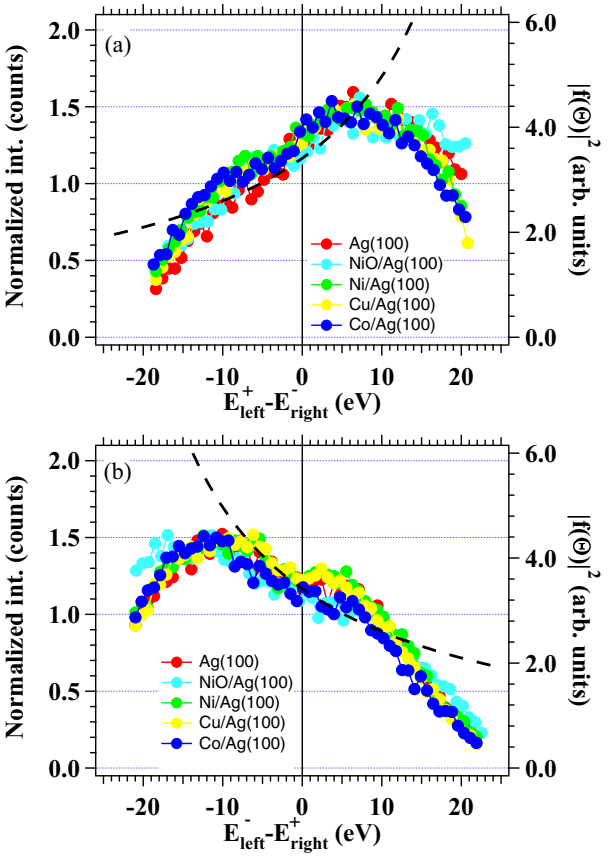

FIG. 5. (Color online) We present the sharing distribution $E^+ - E^-$ using Eq. (4) together with experimental data obtained for different materials during (p,ep) experiments. The normal incidence positron beam has an energy of $E_p = 42$ eV. The sum energy was fixed to 30 ± 2 eV. Panels (a) and (b) are analogous to Fig. 4 as far as which particle is detected by the respective spectrometer. Crystalline samples are the Ag(100) substrate and NiO/Ag(100) films, while Ni, Cu, and Co films are polycrystalline.

In Fig. 4 we present the result for the (p,ep) experiments obtained with $E_p = 42$ eV. The insets highlight the chosen polarity of the spectrometer while the sum energy was fixed to 30 ± 2 eV. As we can see from Fig. 4 the intensity level at the maximum is of the order 1000 counts. Therefore, any selection of the E_{sum} value within a smaller window will cause a significant increase in the statistical noise. Furthermore, we pointed out that the resolution of each spectrometer is 4 eV. This means we cannot expect to reveal finer spectroscopic details by a choice of a smaller E_{sum} window.

We clearly observe asymmetric sharing curves for the (p,ep) process. A comparison with (e,2e) data revealed that the level of instrumental asymmetry can be neglected [10]. Changing the polarity of the spectrometers moves the intensity maximum from the right to the left. In Fig. 4(a) most of the intensity is found for positive x values. This means that, on average, the positron has a higher fraction of the available energy. The intensity maxima of the two (p,ep) sharing curves are observed if the positron has 10 eV more energy than the electron. The intensity minima occur if the electron has a 20-eV higher energy than the positron. The intensity ratio between the two extrema is roughly ≈ 5.

In order to test the generality of the model we investigated also a Ag(100) single crystal and single crystalline NiO, Pd, and Fe films. Additionally, we prepared polycrystalline Cu, Co, Ni, and Fe films. In Fig. 5 we show a selection of the studied samples and compare those with the model sharing curve. As the acquisition time and coincidence count rate is not the same for each material, the maximum intensity for all energy sharing curves was normalized to 1.5. As an example for crystalline samples, we present the data for Ag(100) and NiO films, while the data for Ni, Cu, and Co refer to polycrystalline specimens. Clearly, our model cannot replace a dedicated (p,ep) calculation. Nevertheless, the model calculation predicts a monotonic increase of the intensity as a function of $E^+ - E^-$. For energy sharings $|E^+ - E^-| \leqslant 10$ a rather good agreement to the experiment is given. For larger absolute energy sharing the experimental intensity is below the model calculation.

Despite its simplicity, our scattering model captures the essential aspect of the sharing curves. Obviously, there is only a weak material dependence on the sharing. Ag, Co, and NiO are materials which are, as far as correlation effects are concerned, very different. As a matter of fact, Ag may be regarded as "weakly" correlated material compared to Co and NiO, which display ferromagnetic and antiferromagnetic order, respectively. This means in these materials the electron correlation leads to the emergence of macroscopically

observable effects. NiO is a material usually referred to as "highly" correlated, because the insulating properties are not captured by the usual local density approximation and an additional term (the Hubbard U) has to be included in the theoretical treatment. Despite these large differences the energy sharing curves are very similar. The variation in the electron correlation manifest themselves in the actual coincidence intensity, which we discuss in the last section. The result of Fig. 5 emphasizes the generality of our approach, which rests on the distinguishability of positrons and electrons.

B. Energy distributions for non-normal incidence

The question arises how the previous results are modified if we employ a non-normal incidence geometry. In changing the polar angle θ we also change the mean emission direction from $-45^\circ - \theta$ and $45^\circ + \theta$ according to Fig. 2. The distinguishability of positron and electron is unaffected by the different geometry; hence, we can expect a qualitative similar behavior. From simple symmetry arguments we have to expect an asymmetric sharing curve for an (e,2e) experiment even with normal incidence, but asymmetric emission geometry. Therefore, one could expect an additional contribution which leads to an asymmetric energy sharing in a (p,ep) experiment.

In our studies we set the polar angle to $\theta = \pm 12\ ^\circ$. If the polar angle θ exceeds 30°, one spectrometer will start to be blocked by the surface. Within this range the polar angle can be freely chosen. For a successful coincidence experiment both spectrometers have to be aligned onto the same spot on the sample, additionally the primary excitation has to hit the sample at the same location. An additional constraint occurs if one plans to perform experiments with different polar angles. The excitation spot has to be at the location through which the rotation axis for the polar angle goes. Due to the fact that the excitation source has a diameter of 5 mm, this cannot be strictly fulfilled. This means that the variation of the polar angle leads to a movement of the excitation spot on the sample with a loss in coincidence rate. We identified that for $\theta = \pm 12^\circ$ the performance loss is acceptable.

In Fig. 6 we display the two-dimensional energy distribution from a Ag(100) surface excited with 42 eV positrons. The polar angle θ was chosen to be 12°. The x axis in both cases is the energy scale mapped by the right spectrometer, while the y axis is the energy of the particles detected with the left spectrometer. The solid diagonal line in both plots marks the position of the maximum sum energy $E_{\text{sum}}^{\text{max}}$. Essentially, no intensity is found above this line. Most of the intensity is found within a triangular shaped region near the lower left-hand corner. These events stem from inelastic processes and the energy loss is sufficient to cause the emission of a second electron.

Our instrument is not able to record triple coincidences, but we have detected electron pairs due to positron impact. This strongly suggests the existence of triple emission. These are not included in the theoretical description of (p,ep) and have to be excluded in the analysis if we want to invoke the symmetry of the detection geometry. Via appropriate selection of the sum energy, this can be done and the pair of dashed lines

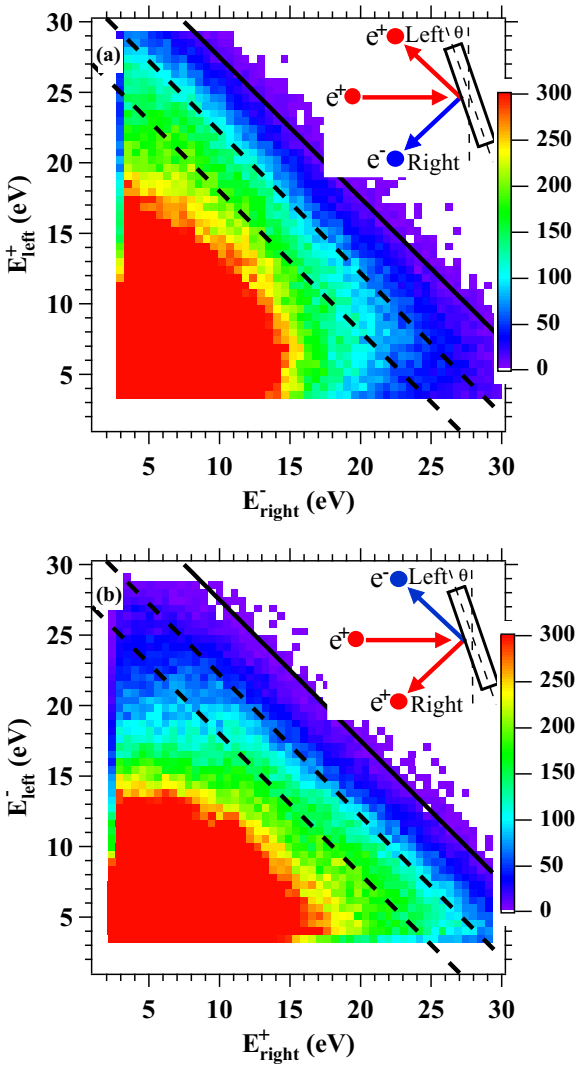

FIG. 6. (Color online) Two-dimensional energy distributions for (p,ep) experiments carried out on Ag(100) crystals with $\theta = 12^\circ$. In both graphs the x and y axes show particle energies detected in the detector right and left, respectively. Insets in each figure indicate which particle (positron or electron) was detect in detectors right and left. Note that this detection was flipped from panel (a) to panel (b). The primary positron beam energy was 42 eV. The solid diagonal line marks the value of the $E_{\text{sum}}^{\text{max}}$, while the dashed diagonal lines indicate the sum energy range used for the sharing curves to be shown below.

indicate the range considered for the computation of the energy sharing curves; see below. The aforementioned asymmetry in the energy distribution can be seen in Fig. 6(a) if we focus on the region marked by the dashed lines. Within this region the intensity is higher in the upper left-hand region compared to the lower right-hand part. We changed the polarities of the spectrometers and observe in Fig. 6(b) that the region of higher intensity is now in the lower right-hand corner. This rules out an instrumental asymmetry and proves the existence of a genuine effect. The dashed lines in Fig. 6 define an energy sum window of $E_{\text{sum}} = 30 \pm 2$ eV. For events in this range we compute the intensity as a function of the energy difference $E_{\text{left}}^{\alpha} - E_{\text{right}}^{\beta}$; see below.

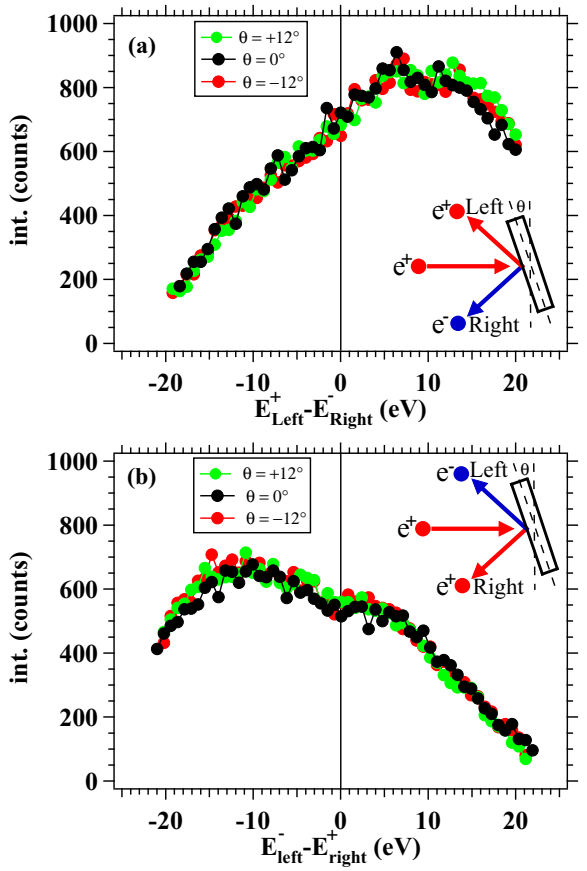

FIG. 7. (Color online) Energy sharing curves obtained by fixing the sum energy to 30 ± 2 eV. The Ag(100) sample was excited by 42 eV positrons. The insets indicate which of the particles is detected by the respective spectrometer.

Focusing on the intensity distribution within the region given by the dashed lines, we notice a movement upon polarity reversal. If we compare this data set with the normal incidence result for Ag(100) surface presented in Fig. 2 of our previous work [10], we hardly see a difference. This can be accentuated by looking at the sharing curves which we present in Fig. 7. These data clearly demonstrate that the outcome of the (p,ep) experiment is not affected by varying the polar angle by 12°. It may have been expected that the distinguishability plays a dominant role and ensures that the positron carries, on average, more energy than the electron. The lack of sensitivity on the polar angle comes as a surprise and is not fully understood. An explanation has to await a proper (p,ep) calculation; however, it is instructive to sketch the basics of the (p,ep) theory for surfaces [8].

In this scheme the initial state is determined by the incoming positron via a LEPD state, while the valence electron is given by a Bloch state. The outgoing positron and electron are presented by time-reversed LEPD and LEED states, respectively. In Eq. (3) we can see how the emitted positron-electron pair determines the valence electron momentum. The kinematically accessible range is given by the angular acceptance and range of the energy window to which the spectrometer have been tuned. According to Fig. 2 both spectrometer cover emission angles are in the range of 30°–60° in normal incidence, while the extreme kinetic energies are 3 and 30 eV, respectively. If the right particle has a kinetic energy of 30 eV and an emission angle of 60°, its in-plane momentum will have a maximum value of 2.43 Å^{-1}. If the counterpart on the left has a kinetic energy of 3 eV and emission angle of 30°, it will possess an in-plane momentum of −0.44 Å^{-1}. This means that in our normal incidence experiments we accept valence states for which $|k_{vb}| \leqslant 1.99$ Å^{-1}. We aligned the sample azimuth such that a high-symmetry direction is within the scattering plane. The Brillouin zone boundary along this direction is at ±1.54 Å^{-1}. This means that in normal incidence we integrate over more than one Brillouin zone. The same considerations can be done for non-normal incidence taking note of Eq. (2). In this case k_{vb} has to be within a window −0.93 to 2.91 Å^{-1} (−2.91 to 0.93 Å^{-1}) for $\theta = 12°$ (−12°). This means we sample an equally large area in the reciprocal space as for normal incidence. Since this area is larger than a Brillouin zone, the available initial states are the same for $\theta = 0°$ or 12° excitation. Therefore, any polar angle dependence is essentially due to the variation of the emission geometry. We point out that we are not able to change the angle of incidence while keeping the emission geometry fixed. Our experimental findings lead us to speculate that the large angular integration effectively removes final-state effects.

C. Intensity relations in normal incidence

Before discussing the material dependence of the coincidence intensity, we like to recall some basic facts of electron and positron emission from surfaces. Readily available excitation sources for surface science are electron or photon sources, which cause the emission of electrons.

In Fig. 8 we display the emission spectra of electrons and positrons for different primary particles from a Ag(100) surface obtained by our apparatus. The polar angle was $\theta = 0°$. In each panel we have added a sketch which highlights the polarity of the incoming and emitted particle. For better comparison of the spectra we scaled the maximum intensity to the value 1. The primary energy of the electron or positron beam was 41 eV. The resolution was the same as for the coincidence experiments, which we quoted to be 4 eV. This is the reason why in all three emission curves the intensity is nonzero at zero kinetic energy. The gray shaded part marks the spectral range covered by our coincidence measurements.

In Fig. 8(a) we present the electron emission spectrum upon electron excitation. The key features are two regions of high intensity usually referred to as secondary and primary peak. Between these two regions the intensity level is lower and may, in principle, contain also Auger electron emission if it is energetically possible to excite a core level. If a primary electron collides with an electron of the surface, it will lose part of its energy. These two electrons may themselves experience further scattering events, leading to a cascade process. This cascade process continues until the primary energy is distributed completely to the electrons. The diffusion of electrons towards the surface with sufficient energy to overcome the vacuum barrier are the cause of secondary electrons. Besides the elastically scattered electrons also electrons with almost the primary energy (quasielastic) are

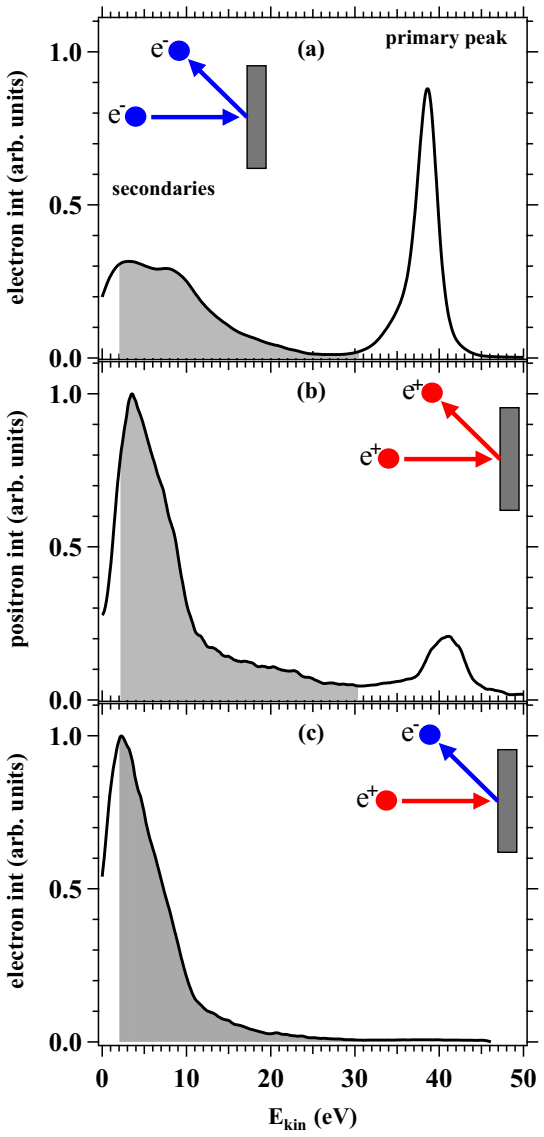

FIG. 8. (Color online) We display the electron emission spectrum due to electron and positron impact in (a) and (c), respectively. The positron emission spectrum due to primary positron excitation is shown in (b). In each case the sample was the Ag(100) surface and the primary beam was aligned along the surface normal. The gray shaded part in each of the spectra marks the energy window covered by our spectrometer during the coincidence measurements.

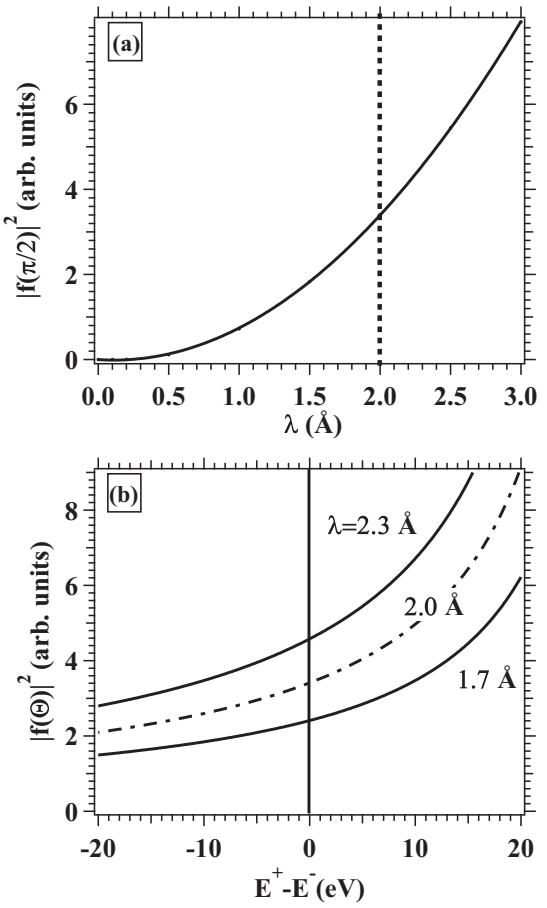

FIG. 9. In (a) we plot the scattering intensity $|f(\pi/2)|^2$ as function of the screening length. The scattering angle $\Theta = \pi/2$ describes equal energy sharing. The dashed vertical line marks the value for λ used for the calculation of the sharing curve shown in Fig. 5. In (b) we present the sharing curve for selected values of λ. The dashed curve is identical to the sharing curve in Fig. 5.

detected, which may have lost part of their energy. The energy loss can de due to the collective excitations like phonons or plasmons, for example.

In Fig. 8(b) we plot the positron emission spectrum upon positron impact. Qualitatively, this spectrum looks very similar to the electron emission spectrum of in Fig. 8(a) in the sense that there exist intensity maxima at both ends of the spectrum. We see an elastic peak which emphasizes the possibility to use positron diffraction LEPD for structural analysis. Therefore, also quasielastic positrons exist which have lost part of their energy via collective excitations. However, the equivalent of a secondary electron does not exist, because for all practical purposes there is only one positron at the time in the sample.

In the case of positron excitation the electron emission spectrum displays the most prominent change in the region near the primary energy; see Fig. 8(c). If the primary particle is a positron, there exist no primary electron peak and therefore the electron intensity near the primary energy is approaching zero. The secondary electron part is not changed dramatically by the different primary particle if we compare the low-energy part of Figs. 8(a) and 8(c). This is reflected by the fact that the average number of electrons emitted per incoming electron is rather similar to the value from positron excitation [37]. This is plausible because in both cases the beginning of the cascade process is due to the collision between two particles with equal mass.

If there were no positron-electron interaction the (p,ep) process would not exist. This suggests that the intensity may be a measure of the interaction strength. Within our scattering model we describe the electron-positron interaction by a screened Coulomb potential. An infinite value of the screening length λ is equivalent to a the bare Coulomb interaction, while the setting $\lambda = 0$ switches off any interaction between the particles. In this sense the parameter λ allows us to effectively tune the correlation strength. In Fig. 9(a) we display the

scattering intensity $|f(\pi/2)|^2$, which refers to equal energy sharing as a function of the screening length λ. The primary energy is set to 30 eV. We see clearly a monotonic increase which is well-described by a quadratic curve. The vertical dashed diagonal line indicates the value for λ used for the sharing curve plotted in Fig. 5.

If the intensity level does depend on the value for λ the question arises how the sharing curve is affected. This is answered by Fig. 9(b), in which the sharing curve is computed for λ in the range 1.7–2.3 Å. The overall shape is hardly changed; only the intensity levels increase. The integrated intensity for $\lambda = 2.3$ Å is about a factor of 2.5 higher than for $\lambda = 1.7$ Å. This reflects the intensity variation seen in the experiment, as presented shortly. At this point we can make the statement that the weak material dependence of the sharing curve and the observed intensity variation are captured within our simple scattering model.

Another consequence is that each scattered positron has an electron counterpart and a positron-electron pair is formed. This means the number of scattered positrons (electrons) generated with a given number of primary particles is identical to the number of positron-electron pairs. The generation rate of pairs is not the same as the detection rate. Besides the finite acceptance angles of the experiment, the generated pairs have to leave the sample before they can be recorded. Low-energy positrons and electrons have a short inelastic mean free path in solids [38,39], which makes them surface sensitive probes. Therefore, the chances to detect one partner of the pair are higher than for the detection of a pair. If this scenario is the dominant process in the emission, the singles rate may show no obvious relation to the coincidence rate.

During a coincidence experiment, we measure three different rates. Besides the positron-electron coincidence count rate, which we can correct for the "random" rate, we determine also the two singles count rate of each spectrometer. With the known primary flux we can determine for each experiment the number of detected electrons (positrons) and positron-electron pairs per incoming positron. We studied the material dependence with normal incidence and a primary energy of $E_p = 42$ eV. We performed two sets of experiments in which one of the spectrometers was tuned for positron detection, while the other was set for electron detection. The averaged values are displayed in Fig. 10, where the y axis refers to the number for positron-electron pairs detected per incoming positron. The x axis is either the number of electrons or positrons detected per incoming positron.

We can see that the pair emission rate for NiO is enhanced by a factor 2–3 compared to the metals. Additionally, we recognize a monotonic relation between the coincidence rate as the function of either singles rate. For the different materials the electron rates vary by a factor of 1.9, while the positron rate scales by a factor of 1.5. Simply put, we can state that a low singles rate results in low coincidence rate. For the same coincidence rate the positron singles rate is about a factor 2–3 smaller than the corresponding electron rate. A primary positron can create secondary electrons with a similar probability as a primary electron [37]. However, a secondary positron cannot be created, because for all practical purposes only one positron at the time is present within the sample.

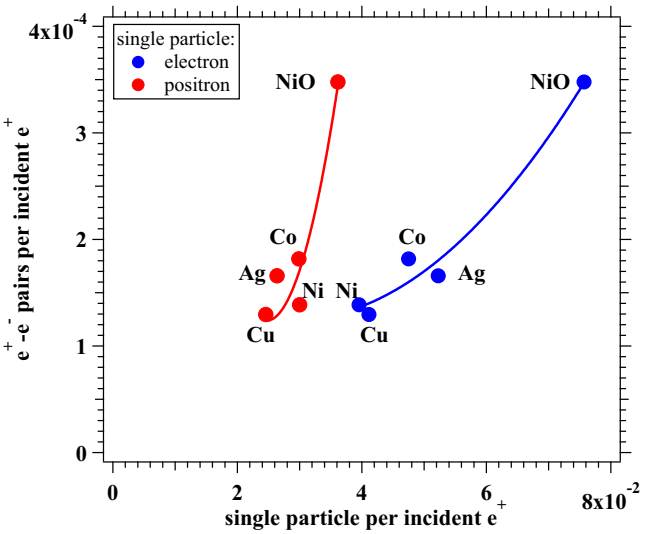

FIG. 10. (Color online) Coincidence count rate as a function of single particle count rate. Note that the count rates are given per incident positron. The red (blue) data points refer to the coincidence rate as a function of positron (electron) rate.

This is a consequence of the possibility of a positron to annihilate with an electron within the sample. Hence, part of the primary flux is lost in this pathway. The result of Fig. 10 clearly demonstrates that the positron-electron pair emission contributes significantly to the single emission rate. A monotonic relation between singles and coincidence rate was also observed in our recent (e,2e) studies on NiO and metal samples [40,41].

Besides the statement that pair emission in (e,2e) and (p,ep) is an efficient emission process, this type of spectroscopy has the potential to determine the correlation strength of matter. A powerful framework in calculating the properties of matter is the local density approximation (LDA). For example the magnetic moment of Fe is in line with the experimental value. However, this theory fails in the description of metal oxides like NiO and CoO. While LDA predicts a metallic phase these materials have a large band gap of a few eV. It turns out that the electron correlation needs to be included in a higher degree of sophistication to explain this fact. This may be regarded as an explanation of why NiO and CoO are termed highly correlated. In this sense the observation of an enhanced coincidence rate of NiO compared to the other materials suggests that the correlation strength can be assessed via the intensity level. Such an interpretation follows from a recent theoretical study dealing with electron pair emission upon photon absorption. It was shown that the pair emission rate is a measure of the correlation strength [42].

V. SUMMARY

We demonstrated that in a positron-electron emission experiment the total available energy is not shared equally between emitted positrons and electrons. This has been observed for a variety of samples. In the studied low primary positron energy range (42–62 eV) the asymmetric energy sharing persists with positrons carrying more energy than electrons.

The observation of such energy asymmetry is a consequence of the distinguishability between positrons and electrons. We found this to be weakly dependent on the investigated material. Qualitatively, the asymmetric energy distribution in (p,ep) experiments was described by a binary scattering model. Comparing the (p,ep) coincidence rate between NiO and several metals, it is proposed that the positron-electron strength increases in strongly correlated materials.

ACKNOWLEDGMENTS

The development of the positron beam greatly benefited from suggestions of R. Krause-Rehberg and P. Coleman. We took advantage of stimulating discussions with H. Gollisch, F. Giebels, and R. Feder. We thank the iThemba LABS team for support and hospitality during the positron source characterization. Funding from the DFG through SFB 762 is gratefully acknowledged.

[1] F. O. Schumann, J. Kirschner, and J. Berakdar, Phys. Rev. Lett. **95**, 117601 (2005).
[2] F. O. Schumann, C. Winkler, and J. Kirschner, Phys. Rev. Lett. **98**, 257604 (2007).
[3] F. O. Schumann, C. Winkler, and J. Kirschner, Phys. Status Solidi B **246**, 1483 (2009).
[4] E. Wigner and F. Seitz, Phys. Rev. **43**, 804 (1933).
[5] J. C. Slater, Rev. Mod. Phys. **6**, 209 (1934).
[6] W. Kohn, Rev. Mod. Phys. **71**, 1253 (1999).
[7] F. O. Schumann, C. Winkler, J. Kirschner, F. Giebels, H. Gollisch, and R. Feder, Phys. Rev. Lett. **104**, 087602 (2010).
[8] F. Giebels, H. Gollisch, R. Feder, F. O. Schumann, C. Winkler, and J. Kirschner, Phys. Rev. B **84**, 165421 (2011).
[9] G. A. van Riessen, F. O. Schumann, M. Birke, C. Winkler, and J. Kirschner, J. Phys.: Condens. Matter **20**, 442001 (2008).
[10] I. S. Brandt, Z. Wei, F. O. Schumann, and J. Kirschner, Phys. Rev. Lett. **113**, 107601 (2014).
[11] J. Berakdar, Nucl. Instrum. Methods Phys. Res. B **171**, 204 (2000).
[12] F. Giebels, H. Gollisch, and R. Feder, J. Phys.: Condens. Matter **21**, 355002 (2009).
[13] R. Krause-Rehberg, N. van der Walt, L. Büttner, and F. Börner, Nucl. Instrum. Methods B **221**, 165 (2004).
[14] P. J. Schultz and K. G. Lynn, Rev. Mod. Phys. **60**, 701 (1988).
[15] H. Bluhme, H. Knudsen, J. P. Merrison, and K. A. Nielsen, J. Phys. B: At. Mol. Opt. Phys. **32**, 5237 (1999).
[16] A. Kövér and G. Laricchia, Phys. Rev. Lett. **80**, 5309 (1998).
[17] F. O. Schumann, R. S. Dhaka, G. A. van Riessen, Z. Wei, and J. Kirschner, Phys. Rev. B **84**, 125106 (2011).
[18] M. Völkel and W. Sandner, J. Phys. E **16**, 456 (1983).
[19] O. Kugeler, S. Marburger, and U. Hergenhahn, Rev. Sci. Instrum. **74**, 3955 (2003).
[20] G. A. Sawatzky, Auger photoelectron coincidence spectroscopy, in *Auger Electron Spectroscopy*, edited by R. P. M. Bryant and C. L. Bryant (Academic Press, San Diego, CA, 1988).
[21] E. Jensen, R. A. Bartynski, S. L. Hulbert, and E. Johnson, Rev. Sci. Instrum. **63**, 3013 (1992).
[22] S. Peacor and T. Hibma, Surf. Sci. **301**, 11 (1994).
[23] J. Wollschläger, D. Erdös, H. Goldbach, R. Höpken, and K. M. Schröder, Thin Solid Films **400**, 1 (2001).
[24] S. Grosser, C. Hagendorf, H. Neddermeyer, and W. Widdra, Surf. Interface Anal. **40**, 1741 (2008).
[25] M. Caffio, B. Cortigiani, G. Rovida, A. Atrei, C. Giovanardi, A. di Bona, and S. Valeri, Surf. Sci. **531**, 368 (2003).
[26] K. Marre and H. Neddermeyer, Surf. Sci. **287-288**, Part 2, 995 (1993).
[27] K. Marre, H. Neddermeyer, A. Chassé, and P. Rennert, Surf. Sci. **357-358**, 233 (1996).
[28] H. Gollisch, N. v. Schwartzenberg, and R. Feder, Phys. Rev. B **74**, 075407 (2006).
[29] U. Rücker, H. Gollisch, and R. Feder, Phys. Rev. B **72**, 214424 (2005).
[30] G. Baym, *Lectures On Quantum Mechanics* (Westview Press, Boulder, CO, 1990).
[31] I. J. Rosenberg, A. H. Weiss, and K. F. Canter, Phys. Rev. Lett. **44**, 1139 (1980).
[32] A. H. Weiss, I. J. Rosenberg, K. F. Canter, C. B. Duke, and A. Paton, Phys. Rev. B **27**, 867 (1983).
[33] X. M. Chen, K. F. Canter, C. B. Duke, A. Paton, D. L. Lessor, and W. K. Ford, Phys. Rev. B **48**, 2400 (1993).
[34] J. Berakdar, S. N. Samarin, R. Herrmann, and J. Kirschner, Phys. Rev. Lett. **81**, 3535 (1998).
[35] S. Samarin, J. Berakdar, O. M. Artamonov, H. Schwabe, and J. Kirschner, Surf. Sci. **470**, 141 (2000).
[36] F. O. Schumann, C. Winkler, and J. Kirschner, Phys. Rev. B **88**, 085129 (2013).
[37] R. Mayer and A. Weiss, Phys. Rev. B **38**, 11927 (1988).
[38] A. B. Denison and H. H. Farrell, Phys. Rev. B **69**, 104302 (2004).
[39] S. Valkealahti and R. M. Nieminen, Appl. Phys. A **35**, 51 (1984).
[40] F. O. Schumann, L. Behnke, C. H. Li, J. Kirschner, Y. Pavlyukh, and J. Berakdar, Phys. Rev. B **86**, 035131 (2012).
[41] F. O. Schumann, L. Behnke, C. H. Li, and J. Kirschner, J. Phys.: Condens. Matter **25**, 094002 (2013).
[42] B. D. Napitu and J. Berakdar, Phys. Rev. B **81**, 195108 (2010).